15165

Medical Imaging

Part 2

Roger H. Schneider, Samuel J. Dwyer III
Chairs/Editors

Proceedings of SPIE—The International Society for Optical Engineering

Volume 767

Part Two of Two Parts

Medical Imaging

Roger H. Schneider, Samuel J. Dwyer III
Chairs/Editors

Sponsored by
SPIE—The International Society for Optical Engineering

Cooperating Organizations
American Association of Physicists in Medicine
Center for Devices and Radiological Health, FDA

1-6 February 1987
Newport Beach, California

Published by
SPIE—The International Society for Optical Engineering
P.O. Box 10, Bellingham, Washington 98227-0010 USA
Telephone 206/676-3290 (Pacific Time) • Telex 46-7053

SPIE (The Society of Photo-Optical Instrumentation Engineers) is a nonprofit society dedicated to advancing engineering and scientific applications of optical, electro-optical, and optoelectronic instrumentation, systems, and technology.

The papers appearing in this book comprise the proceedings of the meeting mentioned on the cover and title page. They reflect the authors' opinions and are published as presented and without change, in the interests of timely dissemination. Their inclusion in this publication does not necessarily constitute endorsement by the editors or by SPIE.

Please use the following format to cite material from this book:
Author(s), "Title of Paper," *Medical Imaging*, Roger H. Schneider, Samuel J. Dwyer III, Editors, Proc. SPIE 767, page numbers (1987).

Library of Congress Catalog Card No. 87-60734
ISBN 0-89252-802-8

Copyright © 1987, The Society of Photo-Optical Instrumentation Engineers. Individual readers of this book and nonprofit libraries acting for them are freely permitted to make fair use of the material in it, such as to copy an article for use in teaching or research. Permission is granted to quote excerpts from articles in this book in scientific or technical works with acknowledgment of the source, including the author's name, the book name, SPIE volume number, page, and year. Reproduction of figures and tables is likewise permitted in other articles and books, provided that the same acknowledgment-of-the-source information is printed with them and notification given to SPIE. **Republication or systematic or multiple reproduction** of any material in this book (including abstracts) is prohibited except with the permission of SPIE and one of the authors. In the case of authors who are employees of the United States government, its contractors or grantees, SPIE recognizes the right of the United States government to retain a nonexclusive, royalty-free license to use the author's copyrighted article for United States government purposes. Address inquiries and notices to Director of Publications, SPIE, P.O. Box 10, Bellingham, WA 98227-0010 USA.

Printed in the United States of America.

MEDICAL IMAGING

Volume 767

Contents

(continued)

(continued)

此为试读,需要完整PDF请访问: www.ertongbook.com

(continued)

(continued)

(continued)

MEDICAL IMAGING

Volume 767

Session 13

Image Processing IV: Cardiology

Chair
Robert A. Kruger
University of Utah Medical Center

A knowledge-based image processing system for the interpretation of coronary arteriograms

Jonathan L. Elion and Steven E. Nissen

Division of Cardiology, University of Kentucky College of Medicine
Room MN670, UKMC, 800 Rose Street, Lexington, Kentucky 40536-0084

Abstract

Although considerable progress has been made in the processing and pattern recognition of medical images, few studies exist on the extension of these methods for processing and interpreting coronary arteriogram. Therefore, we designed and implemented a prototype system for the automated interpretation of coronary arteriograms, using a combination of image processing and knowledge-based methods. Representative frames from a coronary arteriogram are digitized by a video frame-grabber, then a binary representation of the arterial tree created, based on either grey-level thresholding of a single image or pixel variance in the time domain of the sequence. Binary thinning reduces this image to a skeleton, and the coordinates describing the line segments are extracted. These coordinates are read by the knowledge-based interpretive system, implementing an empirical set of facts and rules about coronary anatomy in the PROLOG language. For each arterial segment, the system generates both an anatomic designation and an explanation of the reasoning used for the decision. Quality control is maintained by comparing the interpretations generated to those provided by an experienced angiographer, thereby assuring consistency as the knowledge base is revised and expanded. Current interpretations are based on single-frame static images, with system extensions planned for processing time-variant information (camera panning, changing intensities in a sequence of end-diastolic frames, and segment motion during a cardiac cycle). The system provides not only the basis for computerized interpretation of coronary arteriograms, but also offers an approach for automating the matching of arterial segments in different views, reducing operator interactions during quantitation of coronary stenoses, and tracking arterial motion and position.

Introduction

The field of digital coronary angiography has recovered from an unsteady beginning, and has seen considerable growth and development in recent years. By acquiring arteriographic images in digital format, a wide assortment of computer-based post-processing and analysis routines can be applied. Most forms of quantitative analysis which have been developed to date require operator interaction for the positioning of regions of interest. The computer programs themselves have only a limited a priori knowledge of the structures being imaged, which puts some constraints on the types of automated analysis which are possible. There are two related lines of investigation which have opened up recently in the field of coronary arteriography which provide a motivation for improving the computer's knowledge of the structures it is analyzing. The first involves the imaging of an arterial structure in two orthogonal views, providing full three-dimensional reconstructions of the arterial tree[1], or of coronary lesions[2], and permitting the calculation of the optimal "triple orthogonal" projection (where the x-ray beams in two planes are orthogonal not only to each other but also to the artery being imaged)[3]. The second line of investigation centers on the ability to recognize and track segments of the arterial tree on a frame-by-frame basis, allowing the derivation of descriptors of epicardial vessel motion[4], or to provide computer-identified landmarks for piecewise registration of images[5,6]. Improving the power and complexity of these approaches will require increased sophistication of the computer's ability to automatically recognize characteristics of the coronary arterial anatomy. To demonstrate the feasibility of this avenue of investigation, we therefore designed and implemented a prototype system which provides an automated interpretation of the anatomy of the coronary tree and identification of the anatomic segments, using a combination of image processing and knowledge-based methods.

Methods

The general flow of information through the system is illustrated in Figure 1. A binary representation of the arterial tree is obtained, either by simple gray-level thresholding of a single image, or by the analysis of pixel variance in a sequence of end-diastolic images. The binary representation is thinned to a skeleton (lines are one pixel wide), and the resulting structure decomposed into the coordinate pairs of the line segment endpoints by a tree traversal routine. These coordinates provide the input to the interpretation routine, which consults a knowledge base of normal coronary anatomy,

此为试读,需要完整PDF请访问: www.ertongbook.com

providing interpretations and explanations. These steps are described in greater detail below.

Image processing

The images for this project were taken from simple frames of cineangiographic film from existing clinical studies, and were digitized in a 512 by 512 pixel matrix with 256 levels of gray. The images were processed on a commercial medical image processing system (Kontron Electronics, Mountainview, CA), and end-diastolic images selected for analysis. Where possible, image segmentation was accomplished by simple discrimination of gray levels during maximal opacification with radiographic contrast agent, resulting in a binary image whereby pixels within the boundaries of the opacified coronary artery were represented by white, and all other pixels by black. While this approach resulted in a reasonable facsimile of the arterial tree in several studies, a more sophisticated approach for pixel classification was developed which is better suited to more generalized applications.

The classification scheme used is based on the observation that pixels within a coronary artery tend to have an abrupt rise in intensity early during the image sequence, whereas pixels within myocardial structures have a late rise, and pixels within noncardiac structures remain constant (either bright or dim). By comparing a pixel's statistical variance in a specified time period during the image sequence to a threshold value, it is possible to arrive at a binary classification image. Pixels whose variance exceeds the threshold early in the image sequence are classified as belonging to the coronary arterial structures and are represented by Boolean TRUE (white), while all other pixels are represented by Boolean FALSE (black).

Once a binary representation of the arterial structures is derived, the image is reduced to its pure binary skeleton using traditional thinning procedures. The arterial trees which were used were known to be free from discontinuities, and it was therefore possible to achieve further noise reduction by simply excluding small structures which were found, using a simple size criteria (pixel count).

The final binary skeleton representing the coronary arterial tree was then reduced to the coordinate pairs of the corresponding linear segments that best described the tree. This process was assisted by pre-processing with a 3 x 3 operator which resulted in a numerical descriptor of the connectivity at each point (see Figure 2). Each point in a binary thinned image can be classified as an end point, line point, branch point, or crossing point using this numerical approach (See Figure 3). Starting at the upper left hand corner of the pre-processed binary image (corresponding to the origin of the left main coronary artery), a tree traversal routine "walks" through the binary skeleton, outputting the coordinate pairs of the end-points of each of the segments found. Crossing points were ignored, and assumed to represent crossings in three dimensional space of arterial segments that were not connected.

Knowledge-based interpretation

The computer-generated list of coordinate pairs describing the line segments then became the input for the knowledge-based interpretive system which implemented in an empirical set of facts and rules about coronary anatomy. This task involves a very small search space, as the number of possible arterial segment designations is limited. For the left coronary circulation, the following interpretations were possible: left main, left anterior descending, circumflex, septal, branch of the septal, diagonal, branch of a diagonal, marginal, and branch of a marginal.

A goal-directed approach was taken starting with a search for the arterial segment representing the left main coronary artery, then proceeding to identify segments along the left anterior descending, the circumflex, septals, diagonals, and finally marginal branches. The definition of the left main coronary artery was taken to be the most proximal arterial segment found (closest to the coronary catheter), and, due to the nature of the tree traversal procedure used, was always the first segment in the data base to be analyzed. Next, a search for the arterial segment supplying the left ventricular apex was undertaken, with this segment taken to be part of the left anterior descending coronary artery. The most direct route between the left main coronary artery and the apex was then traced, with all segments contained in the route taken to be members of the left anterior descending artery as well. The remaining arterial segments were then identified using a set of rules which described segment relationships, including connections, branches, and angles. For example, the circumflex coronary artery (in the right anterior oblique projection used) can be thought of as the first branch (at an angle) of the left main coronary artery. Segments defined as belonging to the marginal branches of the circumflex were defined as those which either branched at an angle from the circumflex itself, or formed a branch or continuation of another marginal artery. A representative output from

the system is shown in Figure 4. The coronary tree has been reduced to a set of linear segments, and the endpoints of these lines used as the input to the interpretation routine. A list of the interpretations for each line segment, together with the explanation (corresponding rule) are given. The actual system generates reports listing the coordinates of the lines; these have been replaced here by letter designations for the sake of clarity.

In order to assist with the quality control of the rules used to describe normal coronary anatomy, the arteriograms were first interpreted by a cardiologist, and the true anatomic designation for each segment provided. The program could then double-check its interpretations against the "truth" which was provided by the expert, and any discrepancies reported. As refinements are made in the rule set, it will be possible to request reinterpretation of previously analyzed arteries, to insure that consistency is maintained.

Discussion

While a working prototype system has been demonstrated and holds considerable promise for future developments, there are clearly several limitations to the approach which has been taken. The current system is based on single frame static images, assumes the absence of discontinuities of the arterial segments, and requires that the entire coronary tree be present on a single frame. In reality, diseased coronary arteries frequently demonstrate gaps in opacification, amputations of branches caused by total occlusion proximally, and clipping of the structures against the edge of the imaging frame. Improvements in the image segmentation and tree traversal procedures should help to account for these discrepancies, and should allow the assimilation of multiple end-diastolic frames taken during the panning of the camera. Several alternate approaches for defining the skeleton of the coronary anatomy can be considered, such as segmental edge linking algorithms[7], and the use of computer vision approaches for identification of extended linear structures[8].

The knowledge base itself will be extended to account for anatomic relationships in different views, and to account for known variations of normal relationships. At present, there has been no need to introduce "reasoning under uncertainty"[9], although clinically it is frequently observed that simple anatomic relationships in a static frame may be insufficient to provide unambiguous interpretations of an arterial segment.

In summary, we feel that this system provides not only the basis for computerized interpretation of coronary arteriograms, but also offers an approach for automating the matching of arterial segments in different views, thereby reducing the necessary operator interaction during procedures such as quantification of coronary stenosis, and the tracking of arterial motion and position.

References

1. Pope DL, Parker DL, and Van Bree RE, "Cine 3D Reconstruction of Moving Coronary Arteries from SDA Images", IEEE Computers in Cardiology, October, 1986.
2. Siebes M, D'Argenio DZ, and Selzer RH, "Computer Assessment of Hemodynamic Severity of Coronary Artery Stenosis from Angiograms", Comput Methods Programs Biomed, Vol. 21, pp 143-152, 1985.
3. Wollschlager H, Zeiher AM, Lee P, Solzbach U, Bonzel T, and Just H, "Computed 'Triple' Orthogonal Projections for Optimal Radiological Imaging with Biplane X-ray Systems", IEEE Computers in Cardiology, October, 1986.
4. Perry RA, Wankling PF, and Shiu, "Measurement of Regional Myocardial Shortening by Digitising Routine Diagnostic Coronary Angiograms", IEEE Computers in Cardiology, October, 1986.
5. Goshtasby A, "Piecewise Linear Mapping Functions for Image Registration", Pattern Recognition, in press.
6. Davies DL, Smith PH, and Lintermoza JF, "Discontinuous Registration of Industrial Radiographs Using Profile Analysis and Piecewise Correlations Techniques", Opt.Eng., Vol. 19, pp 425-432, 1980.
7. Eichel PH, Delp EJ, Koral K, and Buda AJ, "A Method for Fully Automatic Definition ofCoronary Arterial Edges from Cineangiograms", IEEE Computers in Cardiology, October, 1986.
8. Astley SM, and Brunt JNH, "Exploitation of Computer Vision Technology in Coronary Cineangiographic Analysis", IEEE Computers in Cardiology, October, 1986.
9. Shortliffe EH, and Buchanan BG, "A Model of Inexact Reasoning in Medicine", Mathematical Biosciences, Vol. 23, pp 351-379, 1975.

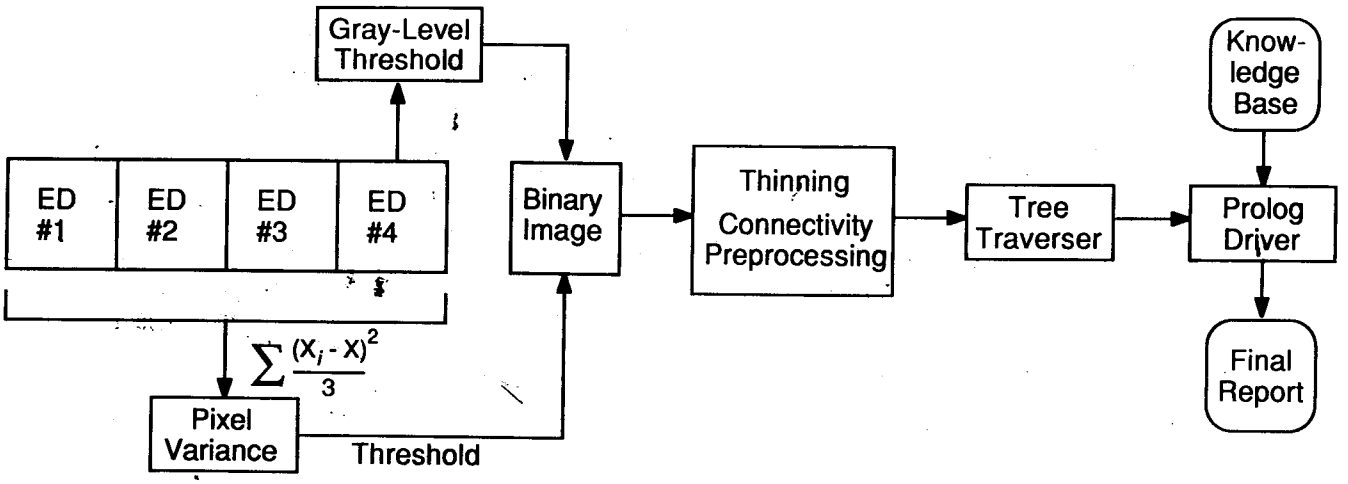

Figure 1: Overall information flow through the system. A binary image corresponding to the arterial tree is created either by analysis of pixel variance over several end-diastolic (ED) frames, or by simple gray-level thresholding of a single frame. The binary image is thinned, then preprocessed using a 3 x 3 connectivity operator. The tree traverser outputs the coordinate pairs of the endpoints of the line segments. Finally, an interpretive driver implemented in Prolog applies the rules about coronary anatomy contained in the knowledge base, and produces the final report.

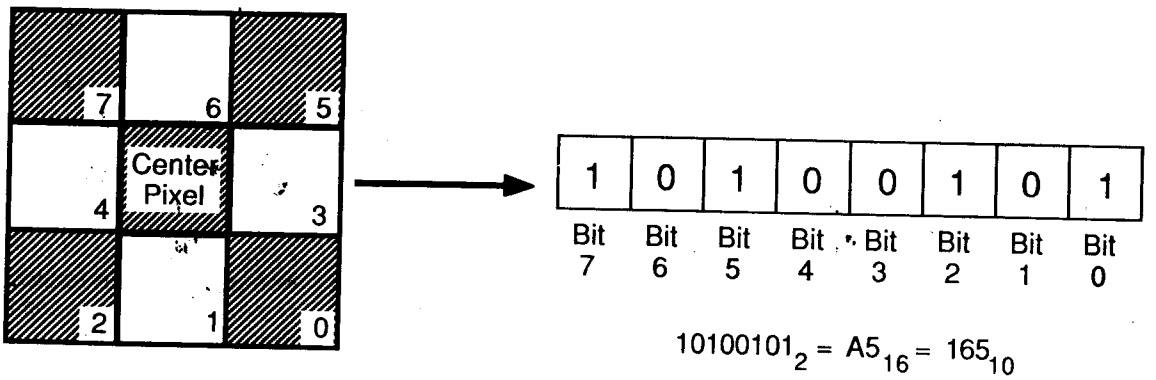

Figure 2: Processing a 3 x 3 connectivity operator. The code assigned to the center pixel is based on the pattern of the eight neighboring pixels, each of which drives the assignment of the corresponding bit in the output value. Pixels which represent Boolean TRUE in the binary image are shown here as shaded squares, with those representing Boolean FALSE shown as open squares.

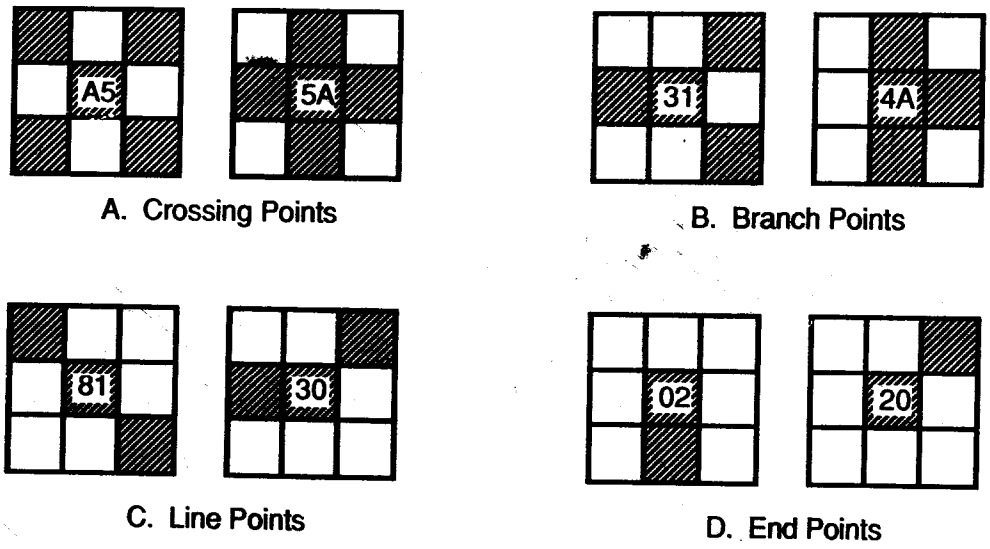

Figure 3: A representative sampling of connectivity types, where the center pixel corresponds to (A) a crossing point; (B) a branch point; (C) a point on the line; and (D) an end point. The corresponding code values which would assigned based on the method shown in Figure 2 are given for each center pixel.

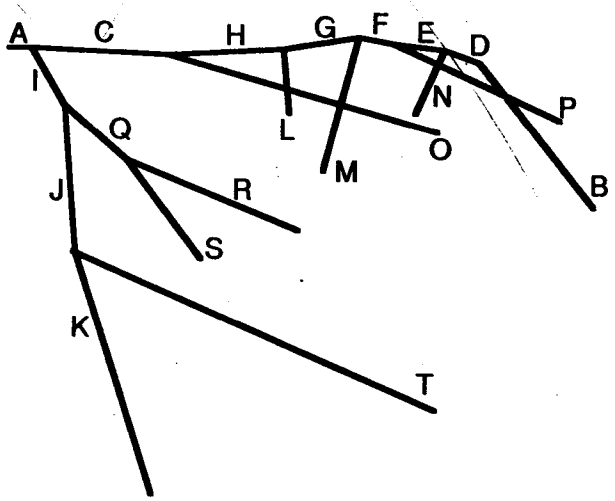

	Interpretation	Explanation
A	Left Main	1st segment in database
B	LAD	Supplies LV Apex
C	LAD	Continuation of Left Main
D	LAD	On route from Left Main to apex
E	LAD	On route from Left Main to apex
F	LAD	On route from Left Main to apex
G	LAD	On route from Left Main to apex
H	LAD	On route from Left Main to apex
I	Circumflex	Branch of Left Main
J	Circumflex	Continuation of Circumflex
K	Circumflex	Continuation of Circumflex
L	Septal	Perpendicular branch of LAD
M	Septal	Perpendicular branch of LAD
N	Septal	Perpendicular branch of LAD
O	Diagonal	Non-perpendicular branch of LAD
P	Diagonal	Non-perpendicular branch of LAD
Q	Marginal	Branch of Circumflex
R	Marginal	Branch or continuation of Marginal
S	Marginal	Branch or continuation of Marginal
T	Marginal	Branch of the Circumflex

Figure 4: Schematic representation of one patient's left coronary anatomy in the right anterior oblique projection, with its associated interpretation. Line segments are identified by letters for clarity, although the system actually reports its results as the coordinates of the line segments. The interpretation (anatomic designation) along with a brief explantion (rule which was applied) are given for each line segment.

Arterial cross-section reconstruction from bi-plane X-ray shadowgraphs

Paul Fenster, Joseph Barba, Manuel Suardiaz, Kenneth K. Wong

Electrical Engineering Department, City College of New York, New York, NY

Edmund M. Herrold, Robert O. Kenet, Jeffrey S. Borer

Department of Medicine, Division of Cardiology, The New York Hospital-Cornell Medical Center, New York, NY

Abstract

An iterative algorithm was used to reconstruct the cross-section of a crescent-shaped vessel lumen. The accuracy of this method was evaluated by comparing reconstruction error in the presence of Gaussian noise of different magnitudes. The sensitivity of the reconstruction algorithm to initial boundary constraint error also was evaluated. Using this algorithm, the reconstruction error was 1.7% when applied to crescent shaped lumen. This error was found to increase significantly with increasing Gaussian noise (error range: 5.75 - 20.75% for noise variance 1-8 pixels^2). Median filtering of the noise-degraded density profiles improved the reconstruction error (error range: 3.25 - 10.5% for noise variance 1-8 pixels^2). The mean reconstruction error was not strongly influenced by initial boundary constraint error. The algorithm provided reasonable reconstruction results when applied to X-ray image derived density profiles of known luminal shapes.

Introduction

Videodensitometric cross-sectional narrowing determined from computer-based digital images of coronary arteries has provided encouraging results as a means of defining luminal cross-sectional area narrowing (1). Unlike the less accurate, less reproducible conventional visual method of assessing coronary stenosis severity (2-4), the videodensitometric approach does not require a priori geometric assumptions (1,5). However, while videodensitometric analysis appears to be of value in defining stenosis severity, additional characterization of the hemodynamic consequences of coronary artery stenoses may be obtainable from definition of arterial cross-sectional shape or contour particulary if this can be done throughout the entire length of the lesion (6,7). Prediction of the hemodynamic effects of lesions may be of value since the presence of turbulence (8) or high shear stresses (9,10) may potentiate the progression of vessel occlusion. Standard single plane angiographic videodensitometry cannot provide such information. Moreover, it has been shown theoretically, that two orthogonal projections of a vessel cross-section (a practical limit for simultaneous views obtained in standard cardiac catheterization laboratories) contain insufficient information for complete reconstruction of all possible luminal cross-sectional shapes (11,12). Therefore, we investigated use of a probability algorithm to iteratively reconstruct an estimate of the cross-section of a vessel lumen, assumed to be homogeneously filled with radiographic contrast agent. The algorithm calculates a probability indicator derived from two orthogonal density profiles of the vessel cross-section obtained from X-ray images. The accuracy of the reconstruction algorithm is examined for a set of initial conditions and noise levels using computer simulations. Reconstructions using actual X-ray shadowgraphs are compared with simulation results.

Methods

Reconstruction Algorithm (Figure 1)

The vessel is assumed to be homogeneously filled with contrast and for the present study the vessel axis is aligned to be orthogonal to the axes of two orthogonal non-simultaneous X-ray beams. The X-ray image photon density is determined by real-time digitization and storage of the logarithmically amplified output of a plumbicon videocamera focused on the output phosphor of the X-ray image intensifier. The X-ray beam intensity is adjusted so that the output is in the linear range of the imaging system. Orthogonal sets of images acquired before and after contrast infusion are subtracted. X-ray photon density profiles of the vessel lumen, are obtained from these background subtracted images. These density profiles are linearly proportional to contrast concentration and depth by the law of Lambert and Beer (13,14). By assuming uniform mixing of contrast, this relation is reduced to a proportionality between contrast depth and X-ray photon density. The X-ray density profile of a vessel cross-section is composed of the background subtracted photon density values for each pixel element. These pixels are positioned on a one pixel wide line across the lumen perpendicular to the vessel axis.

A reference lumen is defined at a nearby reference vessel region. The reference lumen is assumed to be circular and bordered by points where the X-ray density profile equals the background density level. The reference vessel's total X-ray absorption, attributed to the contrast-filled reference lumen, is calculated by integrating the photon density profile perpendicular to the lumen axis. The number of X-ray density units per cross-section pixel, the reference value, is determined from the ratio of this integral and pi times one half the width (radius) of the reference region (in pixels) in the orthogonal view, as

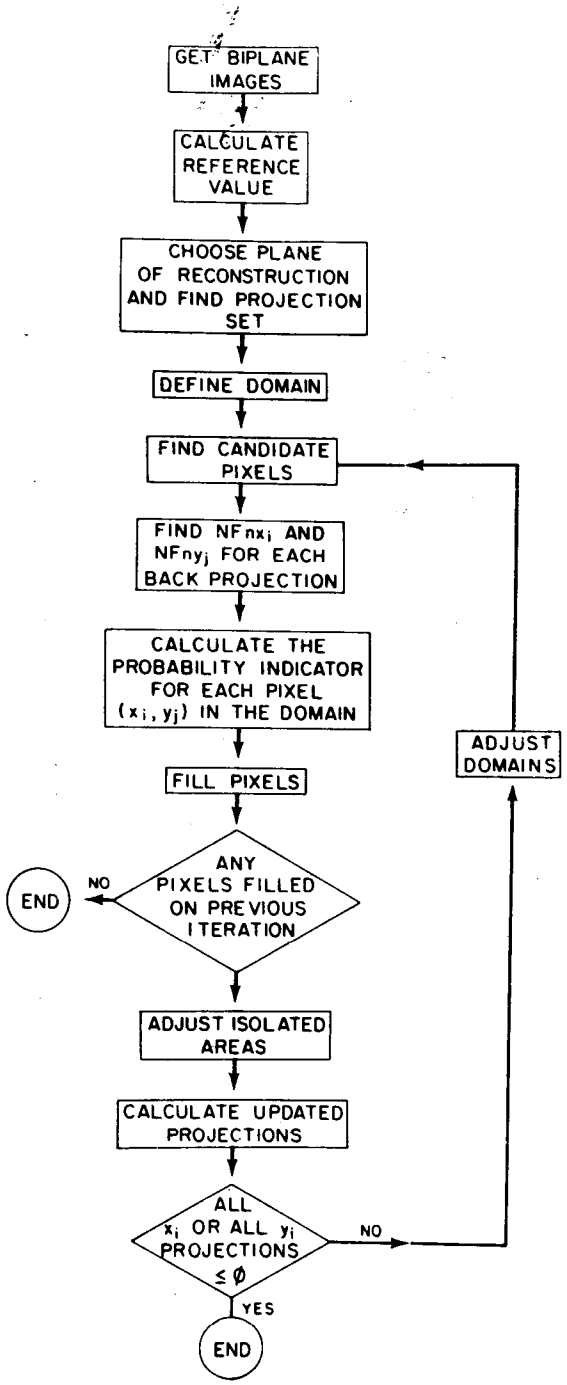

Figure 1: Algorithm Flow Chart

determined by the method of Barba, et al(15).

The outer borders of each cross-section density profile are interactively positioned at the points where the density profile equals the background density level. This is an absolute limit beyond which cross-section reconstruction is not permitted by the algorithm. A reference doman (RD) is calculated and applied to the stenosis reconstruction region by interpolating between circular reference lumen positioned above and below the stenosis. The (circular) RD center and diameter are calculated by interpolating between centers and diameters of these proximal and distal reference lumen . The RD diameter is set one pixel smaller than the interpolated reference diameter in order to bias the reconstruction to fill centrally positioned pixels during the initial reconstruction iteration. On successive iterations, this RD is relaxed slightly (0.5 pixels per iteration) in order to permit construction of lumen borders. The pixels comprising the contrast-filled stenosis lumen are assumed to be a subset of the pixels contained within this superimposed RD.

The two orthogonal X-ray density profiles of the reconstruction plane are the row-sum and column-sum density profiles. The reference value is used to scale the row-sum and column-sum density profiles to cross-section pixel units. The number of pixels contained within the RD in a specific pixel row is defined as the candidate number of pixels for that row. Thus, each row has a limited number of candidate pixels. Similarly, each column has a limited number of candidate pixels. Row-sum and column-sum probability indicators are calculated by dividing the scaled row-sum and column-sum density profiles by the number of candidate pixels for each row and each column, respectively.

Each column is examined to determine the candidate pixel subset (CPS) to be filled as follows. Given a column density value of N pixel units in the column density profile, a maximum of N pixels will be included in the CPS. The N pixels with the highest row probability values are chosen for inclusion in the column CPS. When there are more candidate pixels with equal row probabilities than may be included in the positions remaining in the column CPS (maximum = N) an ambigious situation exists. In order to eliminate the ambigious pixels, the column CPS size is reduced to include only the pixels with unambigious row probability values. Thus, the size of each column CPS is less than or equal to the scaled column density profile. Similarly, each row is examined to determine the row CPS. Assuming a row density value of M pixel units in scaled row density profile, up to M pixels will be included in the row CPS. The M pixels with the highest column probability values are chosen for inclusion in the row CPS. When ambiguous equal probability situations develop, the subset is reduced as in the case of columns. After the row CPS and column CPS pixels have been identified, the intersection of these subsets is chosen as the pixels to be filled. Small unfilled regions bordered by filled candidate pixels are filled and single filled pixels surrounded on all sides by unfilled pixels are emptied in order to eliminate isolated discontinuities which are most likely the result of random noise or ambiguities in the probability profiles. Then, new row-sum and column-sum probabilities are calculated from the remaining row-sum and column-sum density profiles and the number of remaining candidate pixels in each row and column. The RD radius is expanded by a 0.5 pixel increment resulting in a less constrained region and permitting cross-section border reconstruction. Candidate pixels are again considered for filling based on the newly calculated probabilities. This process is repeated iteratively until no more candidate pixels meet all criteria for filling.

The reconstruction algorithm was applied both to simulated ideal density profiles and to X-ray image

此为试读,需要完整PDF请访问: www.ertongbook.com